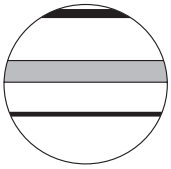

Research Paper

The Holocene
2022, Vol. 32(6) 501–514

DOI: 10.1177/09596836221080758
journals.sagepub.com/home/hol

Early Holocene palaeoceanographic and glaciological changes in southeast Greenland

Camilla S Andresen,[1] Longbin Sha,[2] Marit-Solveig Seidenkrantz,[3] Laurence M Dyke[1] and Hui Jiang[4]

Abstract

Sediment core ER11-16 from Køge Bugt in Southeast Greenland is used to assess early Holocene palaeoceanographic changes and sediment rafting from icebergs calved from the large outlet glaciers in the area. Diatom analysis reconstructs variability in surface water temperature, salinity and sea-ice concentrations, and benthic foraminiferal assemblages is used to reconstruct subsurface ocean conditions. We report Holocene Thermal Maximum in Southeast Greenland during the early Holocene (at least since onset of the record 9100 cal yr BP) until around 4500 cal yr BP, which contrasts with a delay until the mid-Holocene of the Holocene Thermal Maximum in South and Southwest Greenland. The early Holocene warming in Southeast Greenland was caused by a combination of high solar insolation and a weakened subpolar gyre, both of which served to warm the Irminger Current waters subducting onto the shelf. At the same time, the surface temperature was relatively high and sea-ice cover in the polar surface waters of the East Greenland Current was relatively low. High levels of iceberg rafting occurred in Køge Bugt during the early Holocene, synchronously with these warm oceanic temperatures. This is attributed to an increase in iceberg production from the extensive, but retreating, Greenland Ice Sheet. The warm surface conditions were interrupted by a marked and short-lived increase in sea ice around 8200 years ago, providing the first evidence of this global cold episode in Southeast Greenland. After 4500 cal. yr BP, sea-ice cover increased with an expansion of the East Greenland Current, suppressing the inflow of warmer subsurface Irminger Current water to the Southeast Greenland shelf. We relate this oceanic shift to the decreased Northern Hemisphere summer solar insolation. Multi-centennial variability is observed in the grain size spectrum of iceberg rafted debris; a finding we interpret in the context of palaeoceanographic changes.

Keywords

Greenland Ice Sheet, iceberg rafting, Irminger Current, sea ice, Subpolar Gyre

Received 8 September 2021; revised manuscript accepted 14 January 2022

Introduction

Over the last 20 years the accelerated melt and retreat of the Greenland Ice Sheet has prompted concerns about global sea level rise and the stability of thermohaline circulation in a warming world (IPCC, 2021). It has been suggested that the warming of the North Atlantic Subpolar Gyre in the late-1990s, and the associated westward movement of warm water further onto the continental shelf of Greenland, caused marine terminating glaciers in both southeast and West Greenland to thin, retreat and accelerate (Holland et al., 2008; Straneo et al., 2010). In this scenario, changes in atmospheric and oceanic temperatures drive increased subglacial and submarine melt and cause glacier instability (Rignot et al., 2010).

Time series of glacier and ocean conditions are required to understand the influence of oceanographic changes on glacier stability. However, instrumental records from Greenland only cover the last few decades in detail, and the last century at much coarser temporal resolution. Marine sediment cores from around Greenland can be used to reconstruct long-term records of ocean conditions and outlet glacier stability beyond the instrumental time period (Andresen et al., 2012, 2013b, 2014; Wangner et al., 2020; Vermassen et al., 2019a, 2019b) and can cover thousands of years (Andresen et al., 2011, 2013b; Jennings et al., 2002; Ruddiman, 1977; Sheldon et al., 2016; Wangner et al., 2018). In such studies, benthic foraminifera are among the most valuable proxies for determining past ocean conditions at and near the seabed due to these organisms' high sensitivity to bottom-water temperature, salinity, food availability and turbidity (Murray, 1991). In shelf regions, these bottom waters commonly consist of the subsurface water masses characterising the oceans. Analysis of marine diatoms, which are photosynthetic siliceous algae, provides a proxy for understanding past conditions at the sea surface. The distribution of diatom species is largely controlled by ecological and climatic conditions and are especially useful for reconstructing

[1]Department of Glaciology and Climate, Geological Survey of Denmark and Greenland, Denmark
[2]Department of Geography & Spatial Information Techniques, Ningbo University, PR China
[3]Department of Geoscience, Aarhus University, Denmark
[4]Key Laboratory of Geographic Information Science, East China Normal University, PR China

Corresponding author:
Camilla S Andresen, Department of Glaciology and Climate, Geological Survey of Denmark and Greenland, Øster Vold gade 10, Copenhagen K 1350, Denmark.
Email: csa@geus.dk

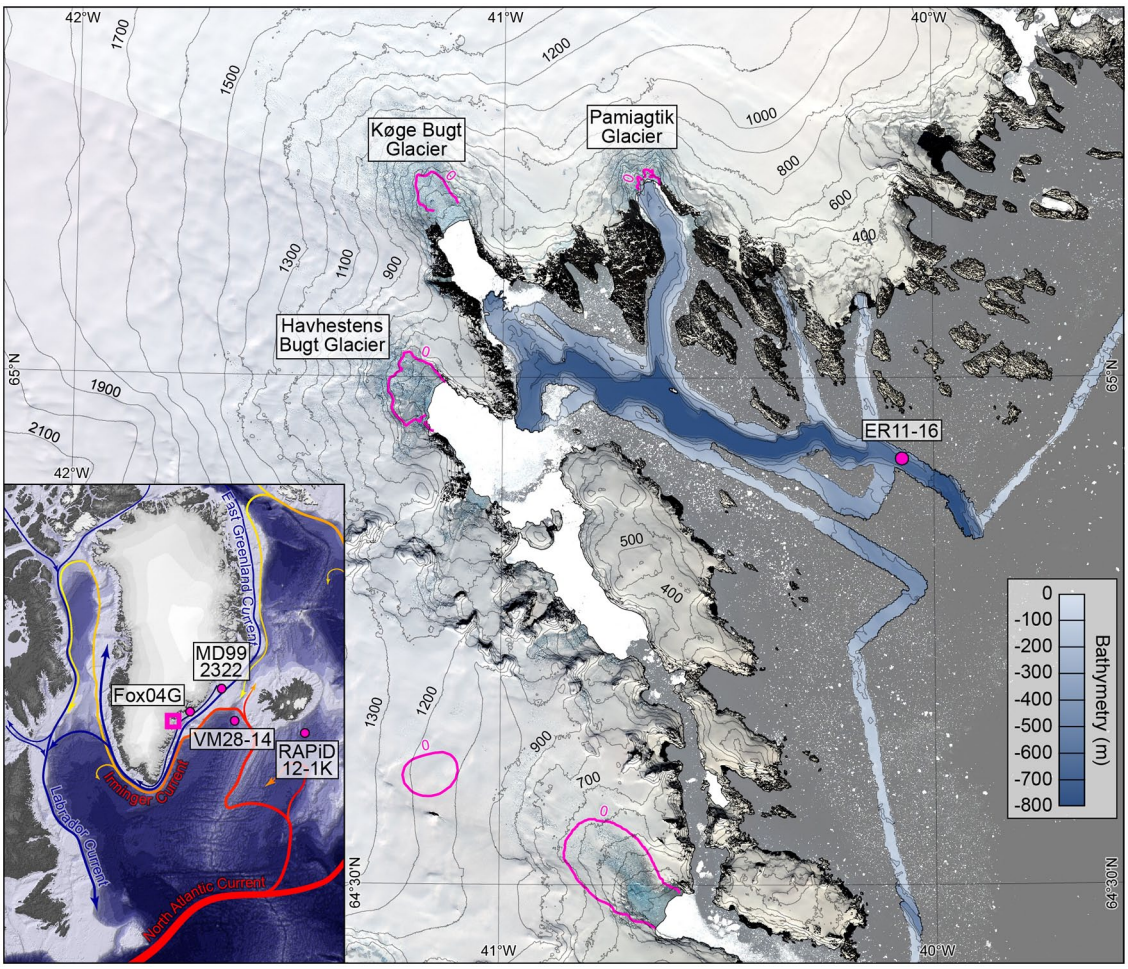

Figure 1. Køge Bugt, southeast Greenland. Landsat 8 imagery (June 2021) is projected onto GIMP surface elevation data with contours shown at 100 m intervals (Howat et al., 2014). The location of the 0 m bed contour (magenta) (Morlighem et al., 2014) is projected onto the ice surface and delineates areas of the ice sheet bed that are below sea-level. Bathymetric data from Dyke et al. (2017) and NASA Ocean Melting Greenland mission (An et al., 2019). The inset map shows generalised ocean surface circulation in southeast Greenland. Core sites for data in Figures 4 and 5 are shown.

variations in surface water temperature, salinity and sea-ice concentration (Medlin and Priddle, 1990; Stoermer and Smol, 1999). Thus, benthic foraminifera and diatom assemblage studies complement each other, and analyses of both these proxies in the same sediment record allow the simultaneous reconstructions of both surface and subsurface oceanographic conditions through time.

Glaciological changes can be reconstructed using the variability in iceberg-rafted debris (IRD) as a measure of iceberg production or glaciological setting (calving glacier vs ice tongue or extensive melange) based on grain size analyses in marine sediment records (Andresen et al., 2011, 2012, 2017). However, the relationship between IRD and glacier activity is complex, and an increase in IRD can potentially be caused by either a glacier advance or by a retreat event (Ekblom Johansson et al., 2020; Funder et al., 1998; McManus et al., 1999). Furthermore, the variability of IRD deposition may, in some cases, also be a function of non-glaciological processes resulting from changes in iceberg transport time, ambient water temperatures, and ocean currents (Andrews, 2000). These complexities highlight that IRD records should be interpreted in the context of climate and palaeoceanographic reconstructions (Vermassen et al., 2019a).

Given the projected warming of the Arctic (IPCC, 2021) there is a need to investigate how glacial systems changed in response to previous warm periods. During the Early- and Mid-Holocene, summers in much of Greenland were 3–5°C warmer than in the mid-20th century, driven by high insolation during the boreal summer (Axford et al., 2021). However, recent efforts to compile records of climate and glacier behaviour in Greenland during the early Holocene highlight that southeast Greenland is a conspicuous blank spot, with no data from this important region (Axford et al., 2021; Briner et al., 2016). Here, we present a record (starting 9100 cal. yr BP) of early-Holocene ocean and glacier changes based on a sediment core from a large marine embayment in southeast Greenland. The age model, foraminiferal analysis, and some of the iceberg rafting reconstruction were previously presented in Dyke et al. (2017) and we here expand on this study by presenting a diatom-based proxy time series of the surface water properties, which includes a proxy for sea-ice occurrence in the upper polar waters of the East Greenland Current. Furthermore, we investigate the grain size composition of iceberg rafted sediment in much greater detail and discuss the palaeoceanographic and glaciological implications of these data.

Study site

Køge Bugt is a large embayment of southeast Greenland, some 40 km long and 20 km wide. The bay hosts several large, marine-terminating outlet glaciers, which drain ice directly from the Greenland ice Sheet (Figure 1). Coarse resolution bathymetric data (Dyke et al., 2017) show the presence of a large elongate depression, more than 600 m deep, running through the centre of Køge Bugt. High-resolution multibeam sonar (Fenty et al., 2016) data show the glacial trough extends from the glaciated coast, through Køge Bugt, and out onto the continental shelf (Millan et al., 2018). Bed topography data (Morlighem et al., 2014) complement these bathymetric data and show that these below sea-level troughs extend inland from the Køge Bugt glacier margins.

However, these troughs extend only a few kilometres inland of the present-day ice margin and the bed topography rises relatively steeply inland from the coast (Figure 1). The geology of the area is composed of Archaean orthogneisses, which form part of the Nagssugtoqidian Mobile Belt (Henriksen and Higgins, 2009).

Surface oceanographic conditions on the continental shelf of southeast Greenland are characterised by the polar waters of the upper East Greenland Current (EGC) and its offshoot the East Greenland Coastal Current (EGCC) (Bacon et al., 2002). These transport cold (0–2°C) and fresh (<33 psu) sea ice-laden surface waters derived from the Arctic Ocean and glacial melt water from East Greenland (Sutherland and Pickart, 2008). The amount of sea ice transported from the Arctic Ocean by these currents varies in timing and distribution, but it is generally observed from spring until September along the coast of southeast Greenland, while locally-formed sea ice/fjord ice prevails in fall to early spring (National Snow and Ice Data Centre, 2012). The coast of southeast Greenland is also characterised by warm (3–6°C), saline (34–35 psu) subsurface waters that originate in the sub-tropical Atlantic (Straneo et al., 2010). These are primarily delivered to the region by the Irminger Current, which forms a limb of the Subpolar Gyre, a large clockwise circulation feature in the North Atlantic (Figure 1), although a minor component of Atlantic-sourced may potentially be derived from Return Atlantic Water and Arctic Atlantic Water, flowing southwards with the East Greenland Current (Quadfasel et al., 1987; Rudels et al., 1994; Schaffer et al., 2017). Locally, this warm Atlantic-sourced water mass penetrates the continental shelf of southeast Greenland beneath a ~250 m thick cap of cold, relatively fresh waters of the EGC and EGCC (Inall et al., 2014; Jackson et al., 2014; Straneo et al., 2010; Sutherland and Pickart, 2008). Although sparse, oceanographic data obtained from instruments attached to diving seals within Køge Bugt show that marine conditions here are similar to further out on the continental shelf. The oceanography of Køge Bugt is thus characterised by a cap of cold polar surface waters and the presence of warm Atlantic water masses at depth (Sutherland et al., 2014). Køge Bugt is filled with icebergs year-round (http://ocean.dmi.dk/arctic/modis.php). Most icebergs are likely of local origin as a chain of islands and shallow seabed to the north of Køge Bugt (Figure 1) prevents icebergs entrained in the southerly flowing EGC and EGCC from entering the embayment (Sutherland and Pickart, 2008).

The occurrence of warm subsurface water on the shelf of southeast Greenland is largely regulated by the dynamics of the Subpolar Gyre, which, in turn, are driven by the North Atlantic Oscillation (NAO) and Eastern Atlantic (EA) dipole patterns (Barnston and Livezey, 1987; Häkkinen et al., 2011). The weakening of the Subpolar Gyre in the late-1990s has been attributed to a shift towards a negative NAO/EA, which is associated with a weaker and more meridional wind stress, that resulted in a contracted and west-ward displaced mode of the Subpolar Gyre (Häkkinen et al., 2011; Hatun et al., 2005; Sarafanov, 2009), and thereby a strengthened Irminger Current flow across the shelf.

Modern observations of the Greenland Ice Sheet show that some of the largest changes in ice dynamics have occurred in the southeast region (Moon et al., 2012). Three outlet glaciers produce icebergs that may transit the study site: Havhestens Bugt Glacier, Køge Bugt Glacier, and Pamiagtik Glacier (Figure 1). Velocity data from these glaciers show that they have exhibited similar patterns of dynamic behaviour over the last two decades as they synchronously accelerated (1999–2003), decelerated (2004–2007) and accelerated again (2008–2012) (Rosenau et al., 2015). The synchronous behaviour of the glaciers in Køge Bugt suggests that they are relatively sensitive and driven by the same primary forcing mechanisms. The velocity data also show that Køge Bugt Glacier is the most active glacier of the three, followed by Havhestens Bugt Glacier, which corresponds to one third to half of the activity of Køge Bugt Glacier (Rosenau et al., 2015). Pamiagtik Glacier is a relatively minor outlet and according to velocity data, it flows more slowly and drains a smaller catchment than the larger glaciers immediately to the south (Rosenau et al., 2015). Consequently, we expect that most icebergs transiting the core site originated from Køge Bugt Glacier and Havhestens Bugt Glacier and we refer to these as the Køge Bugt glaciers.

Information on longer-term glacier changes is provided by Landsat 8 imagery and historical aerial photographs (Korsgaard et al., 2016) and show minor glacial trimlines around the outlet glaciers in Køge Bugt and small moraines close to the present-day margin in land-terminating areas. These features are thought to represent the maximum Little Ice Age (LIA) extent (Kjeldsen et al., 2015), indicating a limited retreat of these glaciers since the LIA maximum. The absence of trimlines and moraines outboard of the LIA margin demonstrates that these areas have likely remained ice-free since deglaciation in the Early Holocene and that the LIA was the largest glacial advance of the Holocene in Køge Bugt (Dyke et al., 2017).

Methods

The 174 cm long core ER11-16 was collected in 2011 from a 595 m deep basin in the centre of Køge Bugt (64.919°N, 40.072°W) approximately 50 km from the present-day ice margin (Figure 1). The core was obtained with a Rumohr corer, without a core catching device; this ensured the preservation of surface sediments and the sediment-water interface. Prior to subsampling, the core was X-rayed at *The Danish National Museum in Brede*, cut in half lengthwise and a line scan image provided using an ITRAX core scanner at *The Globe Institute, University of Copenhagen*. For the study here, a diatom analysis and counts of >2 mm clasts on X-rays were undertaken. The foraminiferal assemblage data, the content of iceberg rafted debris (IRD) in the 63 μm–2mm fraction, and the age model were presented in Dyke et al. (2017), but we here provide a resume of the methods.

Age model

The age model, originally presented in Dyke et al. (2017), is constrained by five ^{14}C dates from benthic calcareous foraminiferal tests in the lower half of the core, and the occurrence of unsupported ^{210}Pb in the surface sample only (Figure 2). Very low concentrations of foraminiferal tests, a common feature in glaciomarine settings, prevented ^{14}C dating of the upper-half of the core. Radiocarbon dates were calibrated with CALIB 7.0 (calib.qub.ac.uk/calib/) using the Marine13 calibration curve (Reimer et al., 2013). The benthic foraminiferal assemblages used for dating indicate an Atlantic water origin, so in accordance with other marine records from the continental shelf of southeast Greenland, a marine reservoir correction of 400 years ($\Delta R = 0$) was applied to all ^{14}C dates (e.g. Andresen et al., 2013a; Jennings et al., 2006, 2011). While Heaton et al. (2020) point out that the Marine20 calibration is uncertain in the Arctic (see also discussion in Pados-Dibattista et al. 2022), we also calibrated the ^{14}C dates using this calibration data set (Table 1) and find that the differences between the two calibration data sets are within uncertainties of the age.

Due to the lack of radiocarbon dating in the interval younger than 6000 years, which is often a challenge in Greenland fjord sediments due to lack of calcareous material, we here focus primarily on the palaeoceanographic and glaciological changes in the early-Holocene. We discuss the younger, poorly-constrained section of the sediment record solely as context for the older sediments.

Diatom analyses

Preparation and counting method. Diatom assemblage analyses were conducted on 1 cm slices of core material taken at 2 cm

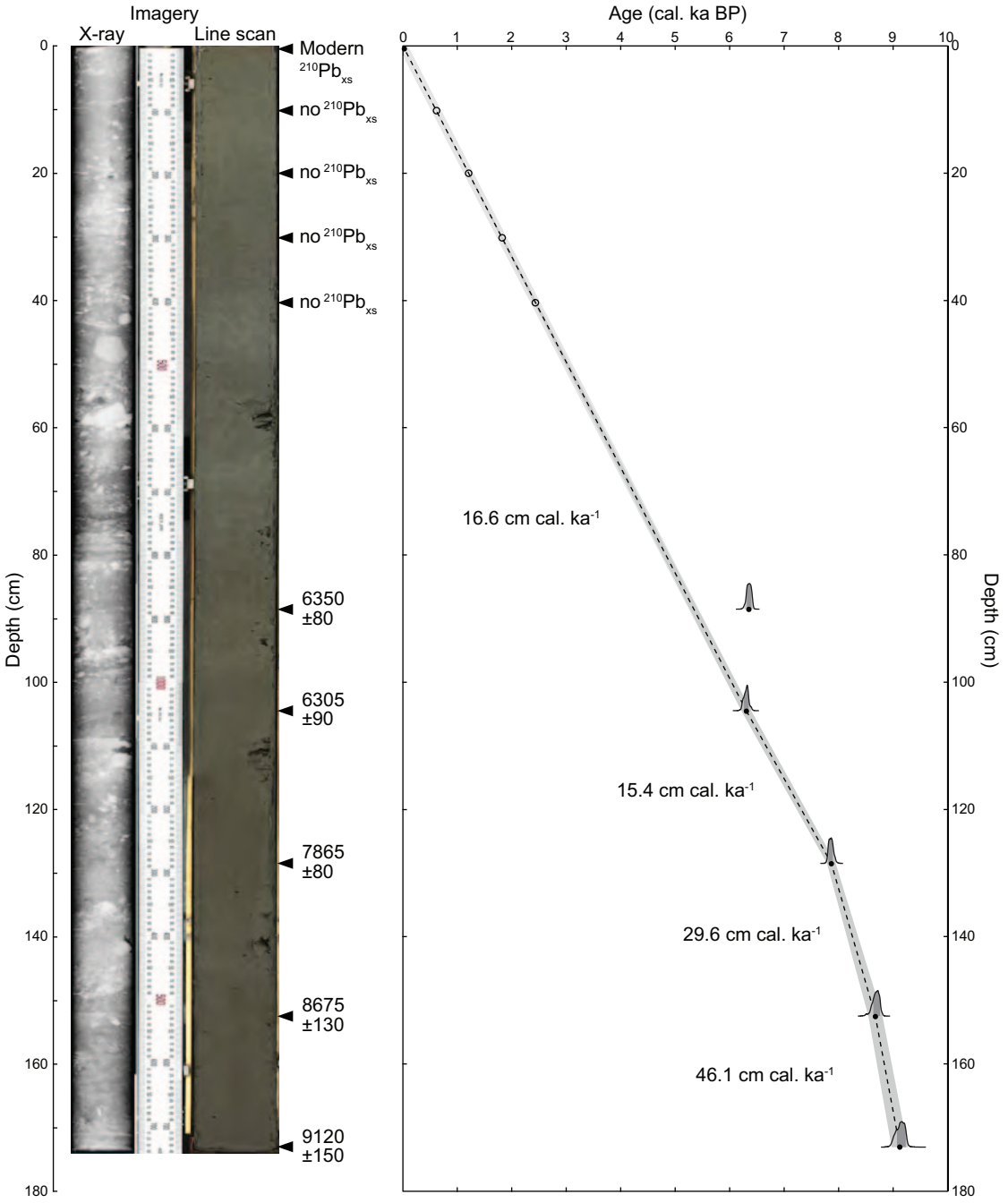

Figure 2. Core description ER11-16. X-ray and line scan images of ER11-16 are shown on a common scale. In the X-ray images white spots indicate denser material such as gravels and sand, while darker parts indicate less dense material such as clay. Black markers next to the line scan image show dated horizons; Radiocarbon ages measured on benthic foraminifera are shown in calibrated years BP with errors of ±2σ.

Table 1. Radiocarbon dates and calibrated ages.

Lab. ID	Depth (cm)	Radiocarbon age (yr BP)	Error (yr)	Median Marine20, $\Delta R = -150 \pm 50$	Error (yr)	Median Marine13, $\Delta R = 0 \pm 50$	Error (yr)
Beta390352	88–89	5940	30	6322	91	6353	61
Beta390353	104–105	5890	40	6269	96	6309	62
Beta387758	128–129	7400	30	7825	86	7862	59
Beta387759	152–153	8180	30	8682	117	8679	97
AAR18323	172–174	8480	55	9093	122	9105	99

intervals from the core. All samples were freeze-dried, and approximately 0.5 g of dry sediment was treated with 10% HCl to dissolve calcareous matter and with 30% H_2O_2 (3 h in a water bath at 70°C) to oxidise organic material. The solution was cleaned with distilled water through a cycle of sedimentation and decantation until no acid was left in the sample. An aliquot of shaken suspension was placed on a cover slip and mixed with a pipette to settle diatoms evenly across the cover slip. After the material had

completely dried, cover slips were transferred onto permanently labelled slides, mounted with Naphrax (refraction index = 1.73) and heated to 250°C. For each sample, at least 300 diatom valves (excluding *Chaetoceros* resting spores) were identified and counted using a Leica microscope at ×1000 magnification. Diatoms were identified to species or species group level following standard taxonomical literature for marine diatoms (Cremer, 1998; Hasle and Syvertsen, 1997; Medlin and Priddle, 1990; Witkowski et al., 2000). A cluster analysis was performed on the diatom percentage data using the program CONISS included in the computer program Tilia 2.6 (Grimm, 1987).

Diatom-based transfer function. Diatoms are useful indicators of surface water conditions in the North Atlantic because they occur widely in marine environments and are highly sensitive to ambient ecological conditions. Surface conditions in the past can be reconstructed by a transfer function to down-core diatom assemblages. The approach has been used successfully for reconstructing past summer sea-surface temperatures (SST) and sea-ice conditions from the high-latitude oceans (Jiang et al., 2015; Justwan and Koc, 2009; Miettinen et al., 2015; Sha et al., 2017). The summer SST transfer function has been developed from a modern calibration dataset consisting of 51 surface sediment samples from around Iceland and Southeast Greenland (Jiang et al., 2001). A weighted averaging with partial least squares regression (WA-PLS) using four components, which yielded a root-mean squared error of prediction of 0.94°C based on the leave-one-out jack-knifing, was employed to quantitatively reconstruct summer SST by using the C2 program (Jiang et al., 2015). In addition, a modern calibration dataset consisting of 72 surface sediment samples from around Greenland and Iceland has been used to develop the April sea-ice concentration transfer function (Sha et al., 2014). The WA-PLS using three components, which has the lowest root-mean squared error of prediction based on the leave-one-out jack-knifing of 1.06 was employed to quantitatively reconstruct the April sea-ice concentration (April SIC) (Sha et al., 2014). Both diatom-based transfer functions, which have been tested by comparing the reconstructed values with instrumental data, have previously been used successfully for reconstructing past summer SST and sea-ice conditions in the North Atlantic region (Jiang et al., 2015; Ran et al., 2011; Sha et al., 2014, 2015, 2016).

Foraminiferal analyses

Foraminiferal assemblage analysis (Dyke et al., 2017) was undertaken on 1 cm slices of core material sampled every 8 cm; additional subsamples were taken at 4 cm intervals at selected levels of the core, where rapid shifts in species composition occur. Samples were wet-sieved, the >63 µm fractions were dried and weighed, and the foraminifera were concentrated by flotation using heavy liquid (CCl4 – density 1.66 g cm^3) separation. Benthic and planktonic species were identified in the >63 µm fraction with approximately 300 species of benthic foraminifera identified from each sample, except in a few levels, where foraminiferal concentrations were low. The percentage of *C. neoteretis*, which is presented here, is calculated as a function of all benthic calcareous. Fluxes of *C. neoteretis* were calculated as number of specimens cm^{-2} yr^{-1}.

Iceberg rafted debris

The occurrence of IRD was determined by analysing the content of sand (63 µm–2 mm fraction) and large clasts (>2 mm) (Andresen et al., 2012; Andrews et al., 1997; Krissek, 1989; St. John and Krissek, 1999). The 63 µm–2 mm grain size composition of the core was measured by wet-sieving 1 cm thick sediment slices, sampled at 2 cm intervals, from the entire core. Next, the annual flux of sand-sized particles to the core site (g cm^{-2} yr^{-1}) was calculated to assess changes in iceberg rafting (Dyke et al., 2017). For the study here, the occurrence of clasts >2 mm was determined by manual counting from the radiographic (X-ray Figure 2) image using a 1-cm, full-width moving window from the full length of the core.

Results

Diatom species distribution

The dominant diatom taxa of the core ER11-16 are *Thalassiosira antarctica* var. *borealis* resting spores, *Thalassiosira antarctica* vegetative cells, *Fragilariopsis cylindrus, Thalassiosira nordenskioeldii, Fragillariopsis oceanica, Bacterosira bathyomphala, Thalassionema nitzschioides, Rhizosolenia hebetata* f. *semispina, Thalassiosira bulbosa, Fossula arctica, Thalassiosira oestrupii* and *Detonula confervaceae* resting spores (Figure 3). *T. antarctica* var. *borealis* resting spores and *T. antarctica* vegetative cells are the most abundant species in the entire record. The diatom record has been divided into three assemblage zones based on the cluster analysis (Grimm, 1987) (Figure 3).

Zone Ia, 9100−8050 cal. yr BP (173−137.5 cm): T. antarctica var. *borealis* resting spores and *T. antarctica* vegetative cells dominate this zone. The warm-water species *T. nitzschioides, T. oestrupii* and *R. hebetata* f. *semispina* are relatively abundant, whereas the percentages of the sea-ice species *D. confervaceae* resting spores, *F. arctica, F. cylindrus* and *T. bulbosa* are low with the exception of abundance peaks in the upper part of zone Ia (Figure 3).

T. antarctica var. *borealis* resting spores is an Arctic neritic taxon found in northern cold-water to temperate regions (Hasle and Syvertsen, 1997; von Quillfeldt, 2000), and it is the main component of the Arctic water diatom assemblage in the North Atlantic (Jiang et al., 2001; Koc Karpuz and Schrader, 1990; Sha et al., 2012).

T. nitzschioides and *T. oestrupii* are the main species of the warm Atlantic water assemblages in the Nordic seas and around Iceland (Jiang et al., 2001; Koc Karpuz and Schrader, 1990), indicating warm sea-surface conditions influenced both by enhanced Atlantic water inflow and surface-water heating (Sha et al., 2012). Therefore, these species can be used here as a measure for the influence of warm Atlantic water masses.

F. cylindrus is a bipolar planktonic species associated with sea ice (Hasle and Syvertsen, 1997), and is the main component of sea-ice diatom assemblages in the North Atlantic (Jiang et al., 2001; Koc Karpuz and Schrader, 1990). *D. confervaceae* resting spores is regarded as a sea-ice taxon in the Laptev Sea (Bauch and Polyakova, 2000; Polyakova, 2001). *T. bulbosa* has been found on sea ice or in the water close to the sea-ice edge (Syvertsen and Hasle, 1984), while *F. arctica* is described as a neritic species connected to sea ice (von Quillfeldt, 1996). These taxa are chief components of the sea-ice diatom assemblage in Køge Bugt, indicating extensive sea-ice cover (Figures 3 and 4h). A short-term sea-ice diatom taxa increase in the upper part of this Zone Ia suggests a period of enhanced sea-ice cover in the study area, taking place around 8200 cal. yr BP.

Zone Ib, 8050−5050 cal. yr BP (137.5−85.5 cm): The diatom assemblage of the zone is very similar to that of Zone Ia and is also dominated by *T. antarctica* var. *borealis* resting spores and *T. antarctica* vegetative cells. It is characterised by a slightly increase in percentage of warm-water species, *T. antarctica* var. *borealis* resting spores, *Fragillariopsis oceanica* and *Thalassiosira hyalina*, coinciding with a continuous decline or even absence of the sea-ice species *D. confervaceae* resting spores, *F. arctica, F. cylindrus* and *T. bulbosa* (Figures 3 and 4h). The similarity between the two zones (Zone Ia and Zone Ib) suggests that

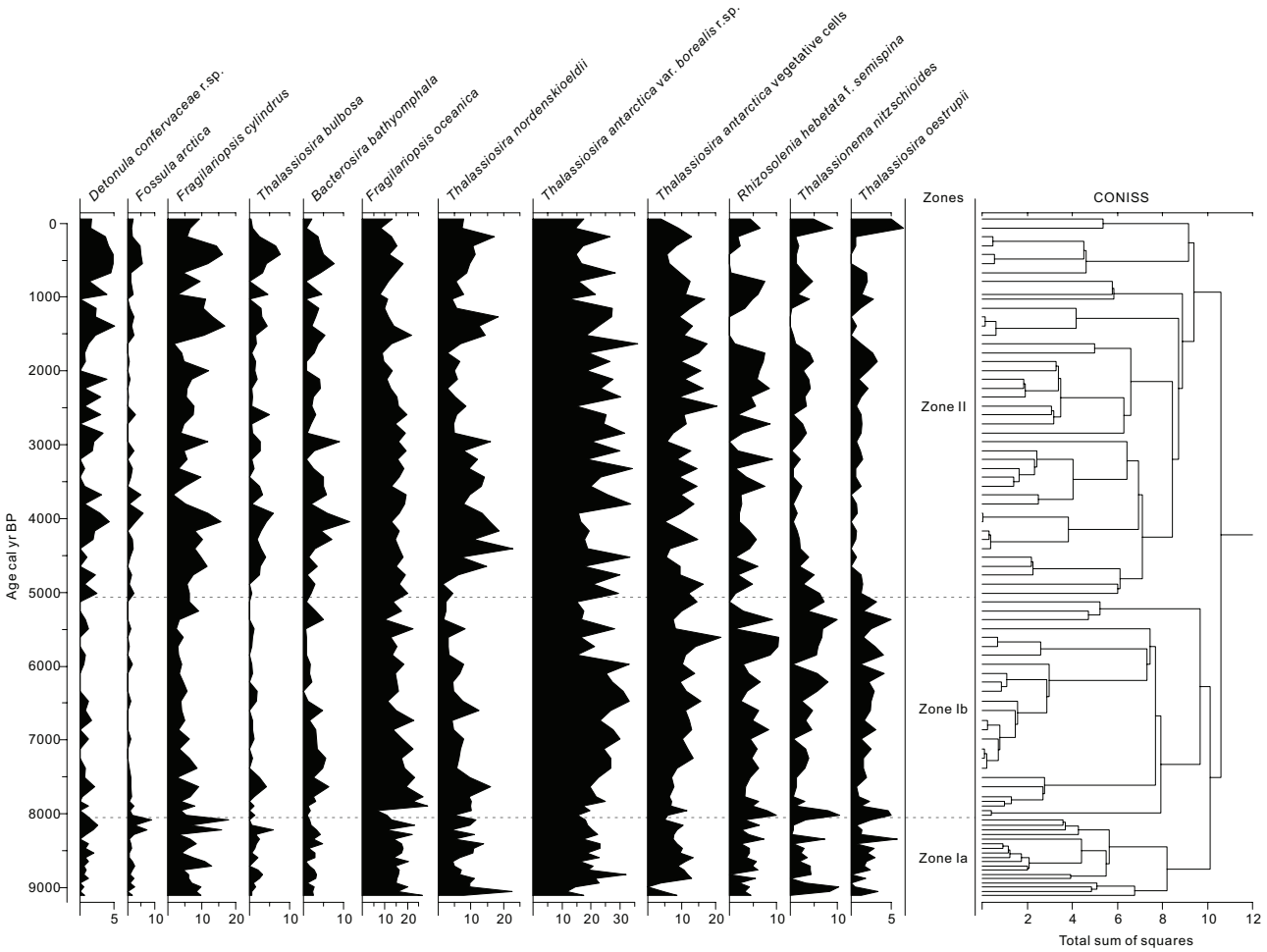

Figure 3. Distribution (percentage, excluding *Chaetoceras* resting spores) of the most common diatoms from core ER11-16. The diatom zonation is based on cluster analysis using the program CONISS included in the computer program Tilia 2.6 (Grimm, 1987).

a relatively warm climate conditions with less sea-ice cover prevailed in Køge Bugt during the early Holocene.

Zone II, after 5000 cal. yr BP (85.5−0 cm): In the younger part of the core, *T. antarctica* var. *borealis* resting spores, *T. antarctica* vegetative cells, *T. nordenskioeldii* and *F. cylindrus* become the dominant species. The main feature of this zone is a significant increase in abundance of sea-ice species *D. confervaceae* resting spores, *F. cylindrus, F. arctica* and *T. bulbosa*, as well as *B. bathyomphala* and *T. nordenskioeldii* (Figures 3 and 4h), which suggest increasingly colder conditions and extended sea-ice cover. In addition, a gradual decline of the warm-water species *T. nitzschioides* and *T. oestrupii* indicates a weakening of the impact of Atlantic water in Køge Bugt.

An increase in the abundance of sea-ice species together with Arctic water species suggests enhanced EGC and more severe sea-ice conditions than for zone I. Moreover, variability in sea-ice species increases and indicates centennial scale episodes of increased sea ice occurrence.

Reconstruction of summer SSTs. The diatom-based transfer funding reconstruction of summer SSTs from core ER11-16 provides a detailed record of changes in sea surface water conditions in Southeast Greenland during the Holocene (Figure 4f). The summer SSTs varies between c. 0.5°C and 3.8°C, with an average value of 2.6°C, and show a general cooling trend during the past 9100 yr. The prediction error for each fossil sample ranges between 0.47°C and 1.16°C. The SSTs were generally above the mean value before 5000 cal. yr BP, except for a short cold period around 8200 cal. yr BP. A marked decrease in summer SSTs began after 5000 cal. yr BP, with SSTs below the mean value for centennial long lasting periods during the last two millennia of the Holocene.

Reconstruction of April sea-ice concentration. The diatom-based transfer function reconstructed April SICs has a total range between 14% and 75%, with variations of more than 60%, showing significant sea-ice changes in Køge Bugt during the Holocene (Figure 4g). The prediction error ranges between 2.86% and 12.1%. Prior to 7700 cal. yr BP, the April SICs were generally 20–50%, with an average of about 38%. Subsequently, the reconstructed April SICs were reduced abruptly to a relatively stable level (ca. 28%) during the period 7700–5000 cal. yr BP, which suggest a generally mild climate with relatively diminished sea-ice prevailed during the Holocene Thermal Maximum in Southeast Greenland. It should be noted that a short-term increase in sea-ice diatom species around 8200 cal. yr BP is not recorded by increased reconstructed April SICs, because the abundance of these diatom species are influenced not only by the April SIC but also the August SIC (Sha et al., 2014). An interval with high values of April SICs from 5000 cal. yr BP to 3000 cal. yr BP was followed by a stepwise decrease after 3000 cal. yr BP. However, in the last two millenia of the Holocene two distinct maximum in April SICs are recorded. According to the age model these maxima takes place c. 1500 cal. yr BP and during the LIA around 500 cal. yr BP, although it should be noted that there are no ^{14}C dates to confirm this.

Foraminifera

The results of the foraminiferal analysis are presented in detail in Dyke et al. (2017). In accordance with similar studies (e.g.

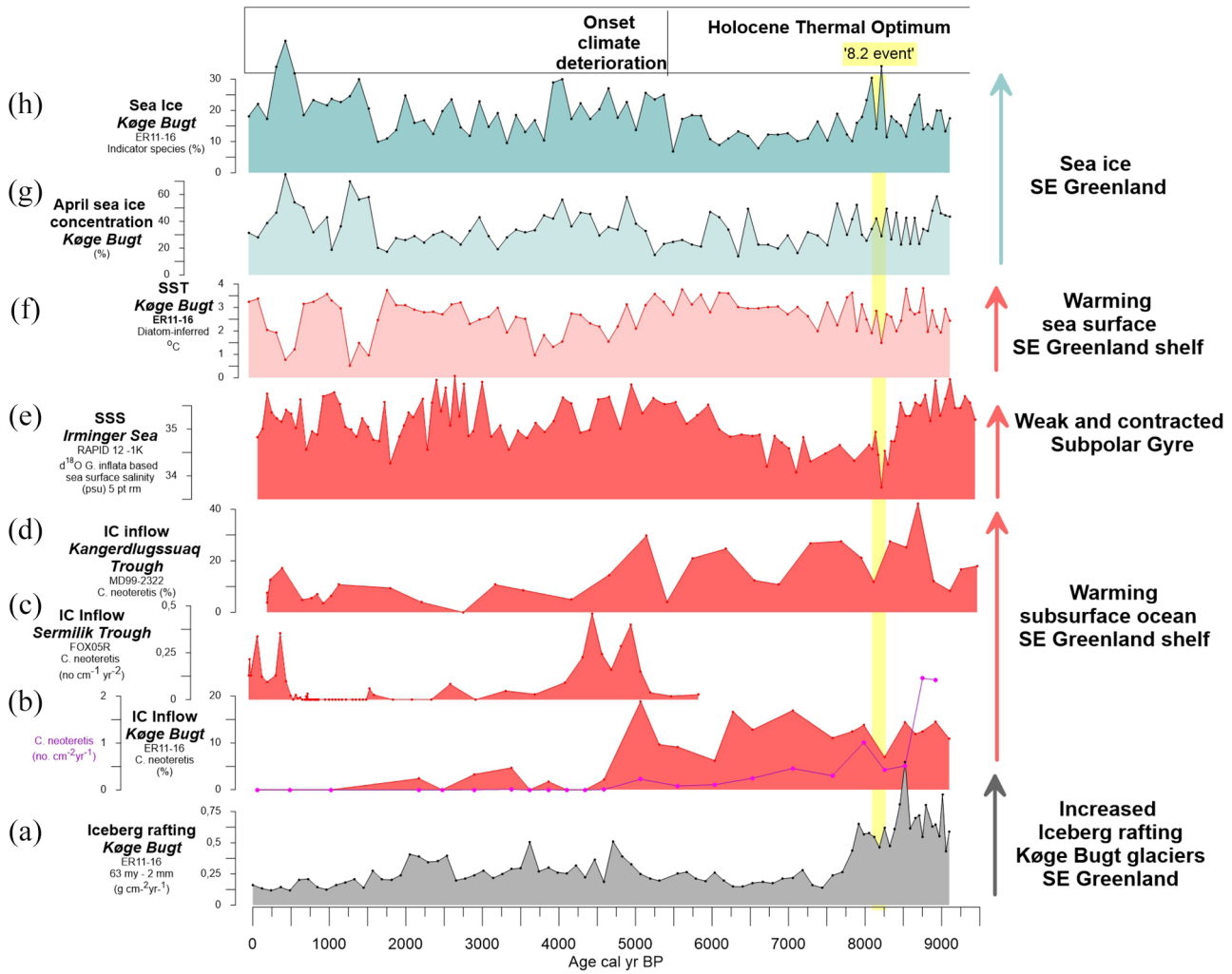

Figure 4. Holocene IRD and ocean record. (a) Flux of sand in ER11-16 indicating relative variability in iceberg rafting in Køge Bugt. (b) Proxies of IC variability from Køge Bugt (ER11-16). Red filled graph: *Cassidulina neoteretis*C %. Purple line: *assidulina neoteretis* flux. (c) Proxy data of IC variability from Sermilik Trough (C. *neoteretis* flux in core Fox04G). (d) Proxy data of IC variability from Kangerdlugssuaq Trough (*C. neoteretis* % in core MD99-2322) (Andresen et al., 2013a; Jennings et al., 2011). (e) Subpolar Gyre variability south of Iceland (salinity reconstruction in core Rapid12-1k Thornalley et al., 2009). (f) Diatom inferred sea-surface temperature (SST) from Køge Bugt (ER11-16). (g) Diatom inferred April sea-ice concentration from Køge Bugt (ER11-16). (h) Sea ice variability from Køge Bugt (ER11-16) calculated from the total percentage of *F. cylindrus, F. arctica, D. confervaceae* resting spore and *T. bulbosa.* The locations of the study sites represented by (c–e) are shown in Figure 1.

Andresen et al., 2013a; Dyke et al., 2017; Jennings and Helgadottir, 1994) we here use *Cassidulina neoteretis* as a proxy for subsurface Atlantic Water inflow (Cage et al., 2021; Jennings et al., 2004; Seidenkrantz, 1995) into the fjords of East Greenland (Figure 4b). The presence of *C. neoteretis* signifies periods when warm, saline Atlantic Water from the Irminger Current reached the sea floor at the core location. Both the percentage and flux data show that the warm water inflow to the trough has varied on Holocene timescales with relatively high and/or warm inflow from the onset of the record around 9000 cal. yr BP until around 4500 cal. yr BP and with a substantial peak in warm water inflow according to flux data between 9000 and 8000 cal. yr BP. After approximately 4500 cal. yr BP the inflow relatively abruptly diminished and remained low for the remainder of the Holocene.

Iceberg rafted debris

The content of sand and large clasts (63 µm–2mm fraction and >2 mm, Figure 5a and b) in core ER11-16 is used as a proxy for iceberg rafting under the assumption that these grains are too large to be carried in suspension within glacial meltwater. Most of the iceberg rafted material likely originates locally from the Køge Bugt glaciers (Dyke et al., 2017) as icebergs from northern regions are unable to enter Køge Bugt due to blocking by islands and shallow bathymetry to the north of the embayment (Sutherland et al., 2014).

The IRD flux of the 63 µm–2 mm fraction was at its highest at the onset of the record in the early-Holocene between 9000 and 8000 cal. yr BP and was relatively low for the remainder of the Holocene, except for multi-centennial episodes in the mid- and late-Holocene with slightly elevated values (Dyke et al., 2017; Figure 5a). Based on the continuous occurrence of IRD in core ER11-16 Dyke et al. (2017) concluded that the glaciers in Køge Bugt were marine-terminating throughout the entire Holocene. This argument is based on the present synchronous behaviour of the glaciers and the assumption that any past retreat of the glaciers onto land would be reflected in the sediment stratigraphy as an interval that is barren of sand and large clasts due to the cessation of iceberg rafting. Instead, only fine sediment suspended in meltwater plume and/or surface run off sediment would be deposited; however, such intervals are not observed in the sediment stratigraphy (Figure 2).

In the present study we compare the 63 µm–2 mm wt% data of Dyke et al. (2017) with our new record of counts of >2 mm grain from the radiographic images and report that these two IRD proxies, sand content and large clasts (Figure 4a and b), in fact does not co-vary. A certain degree of randomness in the grain size

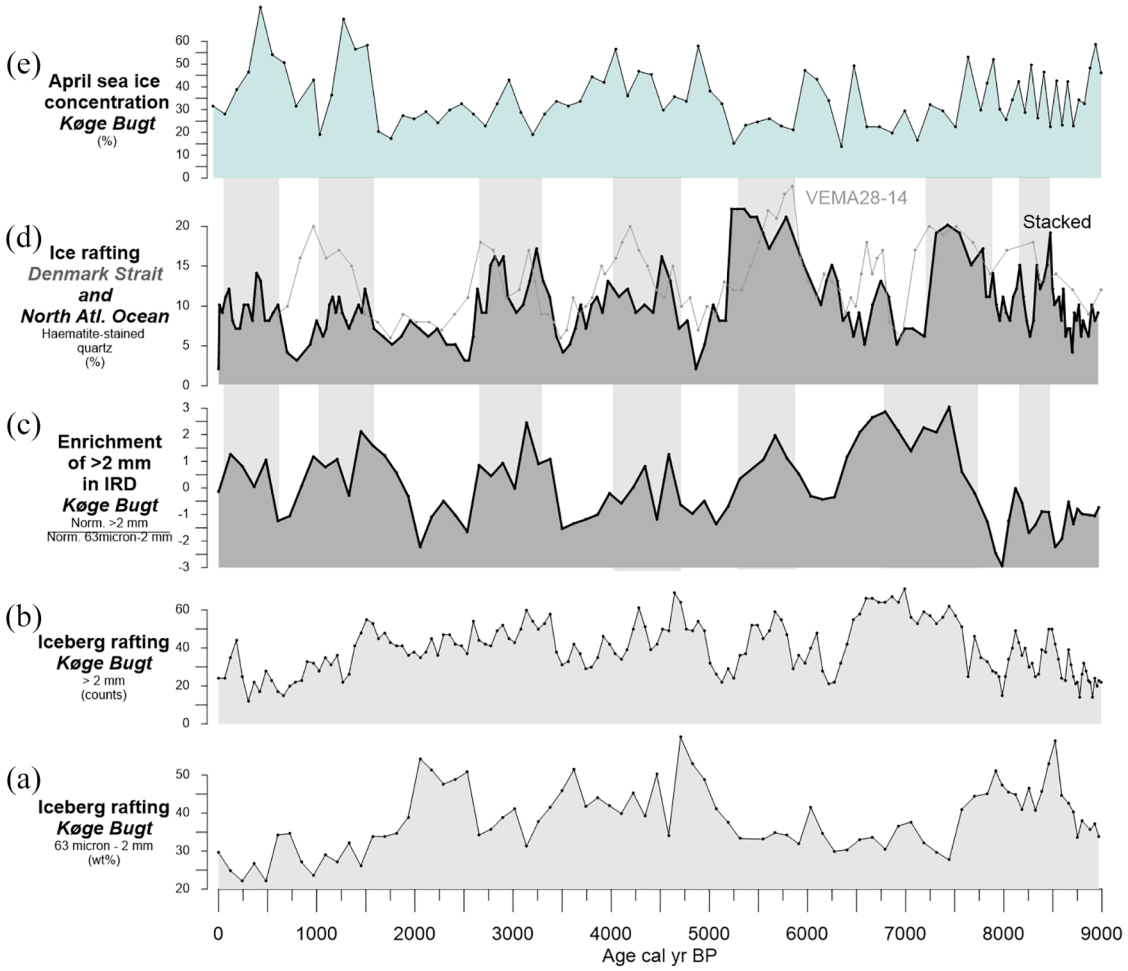

Figure 5. IRD ER11-16. (a) IRD clasts (>2 mm) counted manually from X-ray imagery. (b) The weight of the 63 µm–2 mm fraction as a percentage of the total sediment weight (excluding clasts >2 mm). (c) Normalised clast fraction divided by normalised sand fraction in order show episodes of clast enriched IRD. (d) Sea ice and iceberg rafting records (haematite stained quartz) from the North Atlantic Ocean (stacked) and the Denmark Strait (core Vema28-14) (Bond et al., 2001). (e) Diatom inferred April sea-ice concentration from Køge Bugt (ER11-16).

spectra in IRD is expected (Andrews, 2000), however, the sand and clast content in core ER11-16 vary relative to each other on multi-centennial time scales and does not appear to be sporadic. To emphasise episodes with relatively higher proportion of clasts compared with sand, the two proxies were normalised, and the normalised clast data were divided by the normalised sand data (Figure 5c). This reveals a series of multi-centennial long episodes characterised by delivery of clast-enriched iceberg rafted debris to the core site.

Discussion

Early and mid-Holocene (9000–c. 5000 cal. yr BP) ocean and glacier changes

The Greenland Ice Sheet retreated from its Late Glacial Maximum position to the inner-shelf around 15,000 yr BP in Southeast Greenland (Hughes et al., 2012; Mienert et al., 1992), and reached near its modern position between 12,000 and 10,000 yrs BP (Dyke et al., 2014; Hughes et al., 2012). Studies from East Greenland indicate that maximum air temperatures during the Holocene Thermal Maximum occurred around 10,000 yrs BP, when temperatures exceeded those of the 20th Century in response to high boreal summer insolation (Axford et al., 2017; Levy et al., 2014; Lowell et al., 2013; Vinther et al., 2009). Contrastingly, in south and southwest Greenland the Holocene Thermal Maximum was delayed until the mid-Holocene (Axford et al., 2021; Briner et al., 2016; Larocca et al., 2020a, 2020b; Larsen et al., 2011, 2017). This delay was due to large volumes of cold meltwater from the collapsing northern hemisphere ice sheets entering the North Atlantic, causing substantial surface and upper subsurface water cooling in the Labrador Sea region during the early-Holocene (Jennings et al., 2015; Seidenkrantz et al., 2013; Sheldon et al., 2015). In similarity with southeast Greenland, palaeoceanographic records from south of Iceland show that summer SST was relatively warm here from the onset of the Holocene until 8400 cal. yr BP (Berner et al., 2008; Thornalley et al., 2009; Figure 4e, Van Nieuwenhove et al., 2018), while winters were cool (Van Nieuwenhove et al., 2018). These warm summers are also observable in palaeoceanographic data from southeast Greenland with a notable peak in warm subsurface water around 8800 cal. yr BP in both Køge Bugt and Kangerdlussuaq Trough (Figure 4b and d). This suggests that the Holocene Thermal Maximum occurred earlier in southeast Greenland than in south and southwest Greenland.

It has been suggested that the warming south of Iceland at this time was due to a weakening of the Subpolar Gyre due to large volumes of continuous glacial meltwater suppressing deep-water formation in the Labrador Sea (Thornalley et al., 2009). The weakened subpolar gyre would result in increased inflow of salty waters to south of Iceland (Figure 4e). However, other studies suggest that the warming was also a direct impact of increased

summer solar insolation (Van Nieuwenhove et al., 2018). Modern observations demonstrate that a weakening of the Subpolar Gyre leads to an increase in warm Atlantic subsurface waters on the continental shelf of southeast Greenland (Holland et al., 2008; Straneo and Heimbach, 2013). It is possible that such a mechanism may have resulted in the subsurface ocean warming recorded in our benthic foraminiferal record in Køge Bugt during the Early Holocene. The warming of the subsurface waters, in combination with the high solar insolation, was sufficient to impact on the otherwise cold, fresh surface waters of Køge Bugt as the diatom record demonstrates that this period was characterised by limited sea ice and warmer summer surface temperatures (Figure 4f–h).

The sea ice-indicating diatoms (Figures 3 and 4h) shows a notable increase around 8200 cal. yr BP, suggesting a short episode of increased sea-ice cover interrupting the warm Early Holocene. Similarily, the SST and subsurface records (Andresen et al., 2013b; Jennings et al., 2011) from the Greenland shelf (Figure 4b, d and f) show a minor cooling. This cooling event is likely the expression of the so-called 8.2 ka event, an abrupt global cold interval caused by a reduction in thermohaline circulation. It has been suggested that the collapse in thermohaline circulation was triggered by the catastrophic drainage of glacial Lake Agassiz (Barber et al., 1999) in addition to melt water pulses from a collapsing Laurentide ice sheet (LeGrande and Schmidt, 2008). This cooling may have manifested as intensified sea ice formed locally or exported from the Arctic Ocean with the East Greenland Current.

Keeping in mind that the early Holocene SST warming was likely also caused by high solar insolation on stratified waters, the palaeoceanographic data from Køge Bugt still suggest that glacial meltwater perturbations can cause different responses in the ocean. Both the prolonged SST *warming* from a weakened Subpolar Gyre taking place generally in the early-Holocene (Thornalley et al., 2009), and the abrupt cooling and sea-ice pulse at around 8200 cal. ka BP are thought to be caused by the influx of glacial meltwater into the ocean. The difference between these events is the *rate* of freshwater flux to the ocean and this supports the idea of a strong non-linear response of the climate system to freshwater perturbations of thermohaline circulation (Lohmann and Ditlevsen, 2021).

Iceberg rafting in Køge Bugt was relatively high from the onset of our record to 8000 cal. yr BP (Figure 4a), this occurred synchronously with the intrusion of warm Atlantic subsurface waters into the embayment. We suggest that warm oceanic conditions in this interval destabilised the glaciers in Køge Bugt, resulting in both increased iceberg production and rapid melt-out of IRD at the core site.

The marked intrusion of warm Atlantic-sourced subsurface water on the southeast Greenland shelf lasted until c. 4500 (Figure 4b, d and f). This was accompanied by reduced occurrence of sea ice through this interval (Figure 4g). Warm oceanic conditions and relatively limited sea ice reflect the continuation of warm Holocene Thermal Optimum conditions in the Denmark Strait region (Andresen and Bjorck, 2005; Jennings et al., 2002). However, despite the influx of warm subsurface water, iceberg rafting in Køge Bugt during the Mid-Holocene was markedly lower in comparison with prior to 7800 cal. yr BP (Figure 4a). Data from the DYE ice core located in Southeast Greenland spanning the last 8000 years indicate that the surface of the Greenland Ice Sheet was lowering in response to Holocene climatic and oceanic conditions and did not stabilise close to present-day elevations before 6000 yr BP (Lecavalier et al., 2013). Given the sharp lowering trend from 8000 to 6000 yr BP, and the longer-term adjustment of the Greenland Ice Sheet from a glacial to interglacial configuration, most likely the ice sheet was thinning even faster before 8000 yr BP. Consequently, the decrease in iceberg rafting in Køge Bugt from 7800 cal. yr BP onwards (Figure 4a) likely reflects the start of this transition from rapid thinning and high iceberg production rates to a gradual stabilisation of the Greenland Ice Sheet.

Based on the continuous iceberg rafting seen in core ER11-16, the glaciers draining into Køge Bugt did not retreat onto land at any point during the last 9100 years despite the prolonged warm summers during the Holocene Thermal Maximum (Dyke et al., 2017). Even minor retreats, of a few kilometres at Køge Bugt, Pamiagtik, and Havhestens Bugt glaciers compared to their present position would have resulted in the glaciers reaching a land-based configuration. Dyke et al. (2017) suggested that the unique physical setting of the glaciers was responsible for their continued marine-termination during warm climate and oceanic conditions; the glaciers in Køge Bugt lie on mountainous topography and ice flows into the sea over a relatively steeply-sloping bed. This configuration is inherently stable and allows glaciers to adjust to climatic and oceanic forcing without large retreat events (Robel et al., 2018; Schoof, 2007).

A mid-Holocene climate deterioration (c. 5000 cal. yr BP)

The environmental conditions between 5500 and 4500 cal. yr BP (Figure 4) indicate that this made out the final stage of the Holocene Thermal Maximum in the region. At this time, the higher-than-present summer solar insolation still warmed the surface waters and warm Atlantic-sourced subsurface waters still penetrated onto the continental shelf of southeast Greenland. Similar warm surface waters are also seen in the Labrador Sea (Moros et al., 2006; Sha et al., 2014). However, during the final warm stage of the Holocene Thermal Maximum, the sea-ice cover, as indicated by the diatoms, began to increase around 5500 cal. yr BP (Figure 4g and h). This is synchronous with an increase in the strength of the East Greenland Current (EGC) (Jennings et al., 2002; Perner et al., 2015) and enhanced advection of sea ice through Fram Strait caused by full postglacial flooding of the continental shelves fringing the Arctic Ocean (Bauch et al., 2001). Meanwhile warm Atlantic subsurface waters still reached far north along the coast of West Greenland (Erbs-Hansen et al., 2013; Hansen et al., 2020). Cooling in the Mid- to Late-Holocene was driven by decreased boreal summer insolation (Berger and Loutre, 1991). At the same time iceberg rafting in Køge Bugt increased, and a similar increase in iceberg rafting is also observed in marine cores from further north in East Greenland during this interval (Andrews et al., 1997; Jennings et al., 2002). The increase in iceberg rafting in East Greenland has been attributed to an advance of glaciers from land into the ocean and the onset of iceberg production (Andrews et al., 1997; Jennings et al., 2002). However, as discussed above, the glaciers in Køge Bugt remained in marine terminating settings throughout the Holocene Thermal Maximum (Dyke et al., 2017) and, thus, likely the increase in iceberg rafting in Køge Bugt after 5000 cal. yr BP was caused by the general cooling of Northern Hemisphere climate and a corresponding reduction in ocean surface temperatures. This resulted in reduced iceberg melt rates in Køge Bugt and increased the retention of debris within icebergs before passing over the core site. This scenario is in accordance with Jennings et al. (2002), who suggested that observations of episodic increases in iceberg rafting on the East Greenland shelf in the Late-Holocene were responses to episodic cooling of the surface waters, allowing icebergs to retain their debris for a longer time.

After 4500 cal. yr BP, the subsurface inflow of warm Atlantic Water to the continental shelf of southeast Greenland shelf generally decreased (Figure 4a–c). However, the Subpolar Gyre may still have experienced multi-centennial long-lasting weakening episodes (Thornalley et al., 2009), with contracted episodes of the same magnitude as those in the Early Holocene (Figure 4e). The decrease of warm subsurface inflow to the Greenland shelf after

4500 cal. yr BP was therefore likely due to the intensification of the EGC (Andresen and Bjorck, 2005; Jennings et al., 2002) that led to a thickening of the cold surface water layer and suppressed the inflow of warm Irminger Current waters below this.

Oceanic conditions in southeast Greenland deteriorated further after 2000 cal. yr.BP and the diatom flora shows that the transport of polar water with the EGC intensified and became more persistent. This period included two marked peaks in sea-ice cover, which may have occurred concurrently with episodes of cooler, ice-bearing surface waters penetrating into southerly regions of the North Atlantic around 1500 and 500 cal. yr BP (Figure 5d and e, Bond et al., 2001). This intensification of the EGC was also observed further north in coastal areas of East Greenland (Funder et al., 2011; Perner et al., 2015). The harsher climate after 2000 cal. yr BP was accompanied by a decrease in iceberg rafting and we propose that the intensification of the EGC prevented icebergs from transecting the core site and/or that the cold ocean surface conditions stabilised the glacier and decreased iceberg production.

The interpretations of multi-centennial changes to the iceberg flux presented in this study implies that increased iceberg rafting at a certain geographic location may happen both in response to (i) *colder* periods with glacial advance and/or better retainment of debris in icebergs (as observed after 5000 cal. yr BP) and (ii) *warmer* periods with increased glacier mass loss and iceberg production and/or no sea ice present to trap icebergs (as observed around 9000–8000 cal. yr BP). This apparent contradiction is also mentioned in other IRD studies (Andrews, 2000; Ekblom Johansson et al., 2020; Funder et al., 1998; McManus et al., 1999), which highlights the complexities associated with interpretation of IRD records. For instance, increased air and ocean temperatures can promote faster iceberg disintegration (Davison et al., 2020; Enderlin et al., 2018; Sciascia et al., 2013). Consequently, climate warming can result in decreased retention of IRD within an iceberg as it transits across the continental shelf to the core site. Similarly, periods with colder surface water conditions may preserve icebergs for longer (Dokken and Jansen, 1999; Fronval et al., 1995), eventually spreading IRD over larger regions (Andrews et al., 2014). However, if climatic conditions become too cold then this effect may be reversed; densely packed sea ice can trap icebergs close to glacier fronts, preventing the delivery of IRD to sites further out on the continental shelf (Mugford and Dowdeswell, 2010; Smith and Andrews, 2000; Syvitski and Shaw, 1995). Moreover, changes in climate may affect bedrock erosion by a glacier, which, in turn, affects the debris load of icebergs. Surface meltwater is known to enhance bedrock erosion beneath the margins of the Greenland Ice Sheet (Alley et al., 1997; Cowton et al., 2012; Swift et al., 2002). Consequently, climate induced changes in the production of glacier meltwater may also alter the IRD content in icebergs, however, the exact mechanisms involved in the erosion of bedrock beneath ice sheets are still debated (Jaeger and Koppes, 2015). Altogether these studies highlight, that IRD records should be interpreted cautiously, in the context of oceanographic and climate changes and, if possible, be 'ground-truthed' by comparison with land based observations of glacier changes (Andrews, 2000; Clark and Pisias, 2000; Cofaigh and Dowdeswell, 2001; Syvitski and Shaw, 1995).

Multi-centennial variability in the grain size composition of IRD

Interestingly, despite the unconstrained age model after 6000 cal. yr BP and thus the resultant significant age model uncertainties, we find that multi-centennial episodes of clast-enriched IRD are seemingly synchronous with episodes of more frequent northerly winds and advection of cooler, ice-bearing surface waters in the larger Denmark Strait area; the so-called 'Bond events' (Bond et al., 2001; Figure 5d) and which are regional-scale cooling episodes, that has been linked with solar minima (Bond et al., 2001). A Pearson correlation coefficient was calculated after having interpolated the data from Bond et al. (2001) so that the data points in the two records have the same age and both records were linearly detrended. R values $\geqslant 0.354$ (with $n-2=83$) are statistically significant at the 99.9% level of confidence, implying that a Pearson correlation coefficient of 0.36 between the two datasets shows a synchronous variability at the centennial timescale.

Several scenarios can explain how multi-centennial regional cold periods result in enrichment of clasts in the IRD at the core location in Køge Bugt. Given the lack of field observations to assess the processes influencing debris composition, incorporation, and loss from icebergs (Mugford and Dowdeswell 2010) the possible mechanisms we outline are only tentative explanations, however, we highlight the importance of reporting such findings in case of similar future observations.

We propose that changes in the grain size spectrum in core ER11-16 (Figure 5c) reflect that the IRD is contributed by icebergs derived from *two* glaciers, Køge Bugt Glacier and Havhestens Bugt Glacier (noting that the contribution of icebergs from Pamiagtik Glacier is considered insignificant). We suggest that one of these two glaciers contains a higher proportion of coarse clasts within its IRD, than the other glacier, and that the contribution of IRD to the core site from this glacier changes in pace with regional climatic changes. The two glaciers have slightly different physical settings (Figure 1). This may explain their different contributions to IRD at the core site. Icebergs from Køge Bugt Glacier can drift freely over the core site as local sea ice melts during the summer. Icebergs originating from Havhestens Bugt Glacier have a more complex pathway to the core site. The glacier calves into an enclosed bay; this topographic protection allows fast sea ice to persist longer here, hindering the transit of icebergs away from the glacier front. During colder episodes, the IRD contribution to the core site from Havhestens Glaciers may either *decrease* as icebergs become trapped in the bay and IRD melts out locally, or it may *increase* as the colder climate preserves icebergs and their IRD allowing transit of more debris to the core site.

By reporting these observations of changes in the IRD grain size spectrum and some plausible suggestions to explain them, we hope that future studies will explore the same approach. Maybe changes in the partitioning between clasts and sand in marine sediment cores from other sites near former or current ice sheets also varies in pace with climate change and can be used to discern between various sources. If so, this could hold the key to a better understanding of glacier and ice sheet change over a wide range of time scales.

Conclusions

A sediment-core based palaeoceanographic reconstruction from a marine embayment in Southeast Greenland has been combined with a reconstruction of sediment rafting from icebergs calved off nearby large outlet glaciers. Our analysis shows that IRD changes should be interpreted in the context of longer-term climate changes and grain size distribution, before assigning variability solely to glaciological changes.

The palaeoceanographic reconstruction show that the record of inflow of subsurface Atlantic Water into Køge Bugt, likely primarily from the Irminger Current, compares well with more northerly records from the Southeast Greenland shelf (Jennings et al., 2011) and the wider Irminger Sea region (Andresen et al. 2004, 2005, 2006, 2007) and show warm conditions during the Early Holocene and the Holocene Thermal Maximum. At the same time sea-ice cover was relatively low except for a short-lived peak around 8200 years ago, and altogether this reflects the high summer solar

insolation of the Early Holocene. Exceptionally warm IC inflow between 9000 and 7800 cal. yr BP, as also observed elsewhere in the Irminger Sea (e.g. Van Nieuwenhove et al., 2018), was likely related to the combined effect of the high summer solar insolation and an overall weakening of the Subpolar Gyre due to decreased thermohaline circulation (Thornalley et al., 2009; Van Nieuwenhove et al., 2018). The high solar insolation and influx of warm subsurface water caused intensified melting of the Greenland Ice Sheet (e.g. Van Nieuwenhove et al., 2018) and indeed our Southeast Greenland record shows the highest iceberg rafting at this time. During the Holocene Thermal Maximum, the Greenland ice sheet had eventually lowered from its Glacial elevated position to its current at c. 6000 cal. yr BP, and we suggest that this is the cause of a relatively low iceberg production and IRD flux during this time.

After c. 5000–4500 cal. yr BP, subsurface inflow of warm Atlantic-sourced water to the Southeast Greenland shelf decreased and we propose that this was due to the concurrent intensification of transport of Polar Water with the East Greenland Current (EGC), driven by a decrease in northern hemisphere insolation. This intensification of Polar Water transport may have resulted in a thickening of the EGC and thus suppression of the Irminger Current inflow. The colder surface ocean conditions allowed icebergs to retain their debris for a longer time explaining the observed increased iceberg rafting. Contrary, after 2000 cal. yr BP iceberg rafting decreased in response to concurrent further intensification of the EGC, which prevented icebergs from transecting the core site and/or increased mass balance of the glacier and decreased iceberg production.

Finally, we report multi-centennial episodes of clast-enriched IRD that are synchronous with episodes of colder climate in the larger Denmark Strait area (Bond et al., 2001) and propose this may reflect different setting of the two glaciers.

Funding

The author(s) disclosed receipt of the following financial support for the research, authorship, and/or publication of this article: This work was supported by the Danish VILLUM Foundation (grant number 10100 to CSA) with further support from by the National Natural Science Foundation of China (Grant Nos. 41776193, 41876215 and 42176226) to SL. This work was also supported the Danish Council for Independent Research (grants no. 7014-00113B (G-Ice) and 0135-00165B (GreenShelf)) and the European Union's Horizon 2020 research and innovation program under grant agreement No. 869383 (ECOTIP) to MSS.

ORCID iDs

Camilla S Andresen https://orcid.org/0000-0002-5249-1812

Marit-Solveig Seidenkrantz https://orcid.org/0000-0002-1973-5969

References

Alley RB, Shuman CA, Meese DA et al. (1997) Visual-stratigraphic dating of the GISP2 ice core: Basis, reproducibility, and application. *Journal of Geophysical Research: Oceans* 102: 26367–26381.

An L, Rignot E, Chauche N et al. (2019) Bathymetry of southeast Greenland from oceans melting Greenland (OMG) data. *Geophysical Research Letters* 46: 11197–11205.

Andresen C, Hansen M, Seidenkrantz M-S et al. (2013a) Mid- to late-Holocene oceanographic variability on the southeast Greenland shelf. *The Holocene* 23(2): 167–178.

Andresen CS and Bjorck S (2005) Holocene climate variability in the Denmark Strait region - a land-sea correlation of new and existing climate proxy records. *Geografiska Annaler* 87: 159–174.

Andresen CS, Björck S, Bennike O and Bond G (2004) Holocene climate changes in southern Greenland: evidence from lake sediments. *Journal of Quaternary Science: Published for the Quaternary Research Association* 19(8): 783–795.

Andresen CS, Björck S, Jessen C, and Rundgren M (2007) Early Holocene terrestrial climatic variability along a North Atlantic Island transect: palaeoceanographic implications. *Quaternary Science Reviews*, 26(15–16): 1989–1998.

Andresen CS, Björck S, Rundgren M, CONLEY DJ and Jessen C (2006) Rapid Holocene climate changes in the North Atlantic: evidence from lake sediments from the Faroe Islands. *Boreas*, 35(1): 23–34.

Andresen CS, Bond G, Kuijpers A, Knutz PC and Björck S (2005) Holocene climate variability at multidecadal time scales detected by sedimentological indicators in a shelf core NW off Iceland. *Marine Geology*, 214(4): 323–338.

Andresen CS, Kokfelt U, Sicre M-A et al. (2017) Exceptional 20th century glaciological regime of a major Southeast Greenland outlet glacier. *Scientific Reports* 7(13626): 1–8.

Andresen CS, McCarthy DJ, Valdemar Dylmer C et al. (2011) Interaction between subsurface ocean waters and calving of the Jakobshavn isbræ during the late Holocene. *The Holocene* 21(2): 211–224.

Andresen CS, Schmidt S, Seidenkrantz M-S et al. (2014) A 100-year record of changes in water renewal rate in Sermilik Fjord and its influence on calving of Helheim Glacier, Southeast Greenland. *Continental Shelf Research* 85: 21–29.

Andresen CS, Sicre M-A, Straneo F et al. (2013b) A 100-year long record of alkenone-derived SST changes by southeast Greenland. *Continental Shelf Research* 71: 45–51.

Andresen CS, Straneo F, Ribergaard MH et al. (2012) Rapid response of Helheim Glacier in Greenland to climate variability over the past century. *Nature Geoscience* 5: 37–41.

Andrews JT (2000) Icebergs and iceberg rafted detritus (IRD) in the North Atlantic: Facts and assumptions. *Oceanography* 13: 100–108.

Andrews JT, Bigg GR and Wilton DJ (2014) Holocene ice-rafting and sediment transport from the glaciated margin of East Greenland (67–70°N) to the N Iceland shelves: Detecting and modelling changing sediment sources. *Quaternary Science Reviews* 91: 204–217.

Andrews JT, Smith LM, Preston R et al. (1997) Spatial and temporal patterns of iceberg rafting (IRD) along the East Greenland margin, ca. 68°N, over the last 14 cal.ka. *Journal of Quaternary Science* 12: 1–13.

Axford Y, de Vernal A and Osterberg EC (2021) Past warmth and its impacts during the Holocene thermal maximum in Greenland. *Annual Review of Earth and Planetary Sciences* 49(1): 279–307.

Axford Y, Levy LB, Kelly MA et al. (2017) Timing and magnitude of early to middle Holocene warming in East Greenland inferred from chironomids. *Boreas* 46: 678–687.

Bacon S, Reverdin G, Rigor IG and Snaith HM (2002) A freshwater jet on the east Greenland shelf. *Journal of Geophysical Research: Oceans* 107(C7): 5–1.

Barber DC, Dyke A, Hillaire-Marcel C et al. (1999) Forcing of the cold event of 8200 years ago by catastrophic drainage of Laurentide lakes. *Nature* 400: 344–348.

Barnston AG and Livezey RE (1987) Classification, seasonality and persistence of low-frequency atmospheric circulation patterns. *Monthly Weather Review* 115: 1083–1119.

Bauch HA, Erlenkeuser H, Spielhagen RF et al. (2001) Lithology, micropaleontology and isotope record of sediments from the Nordic Seas. PANGAEA, https://doi.org/10.1594/PANGAEA.735161, Supplement to: Bauch HA et al. (2001): A multiproxy reconstruction of the evolution of deep and surface waters in the subarctic Nordic seas over the last 30,000 years. *Quaternary Science Reviews* 20(4): 659–678.

Bauch HA and Polyakova YI (2000) Late-Holocene variations in Arctic shelf hydrology and sea-ice regime: Evidence from north of the Lena Delta. *International Journal of Earth Sciences* 89: 569–577.

Berger A and Loutre MF (1991) Insolation values for the climate of the last 10 million years. *Quaternary Science Reviews* 10: 297–317.

Berner KS, Koç N, Divine D, Godtliebsen F and Moros M (2008) A decadal-scale Holocene sea surface temperature record from the subpolar North Atlantic constructed using diatoms and statistics and its relation to other climate parameters. *Paleoceanography* 23(2).

Bond G, Kromer B, Beer J et al. (2001) Persistent solar influence on North Atlantic climate during the Holocene. *Science* 294: 2130–2136.

Briner JP, McKay NP, Axford Y, Bennike O, Bradley RS, de Vernal A, Fisher D, Francus P, Fréchette B, Gajewski K, Jennings A, Kaufman DS, Miller G, Rouston C and Wagner B (2016) Holocene climate change in Arctic Canada and Greenland. *Quaternary Science Reviews*, 147: 340–364.

Cage AG, Pieńkowski AJ, Jennings A et al. (2021) Comparative analysis of six common foraminiferal species of the genera *Cassidulina, Paracassidulina*, and *Islandiella* from the Arctic–North Atlantic domain. *Journal of Micropalaeontology* 40: 37–60.

Clark PU and Pisias NG (2000) Interpreting iceberg deposits in the deep sea. *Science* 290: 51–52.

Cofaigh CÓ and Dowdeswell JA (2001) Laminated sediments in glacimarine environments: Diagnostic criteria for their interpretation. *Quaternary Science Reviews* 20(13): 1411–1436.

Cowton T, Nienow P, Bartholomew I et al. (2012) Rapid erosion beneath the Greenland ice sheet. *Geology* 40(4): 343–346.

Cremer H (1998) The diatom flora of the Laptev Sea (Arctic Ocean). *Bibliotheca Diatomologica* 40: 5–169.

Davison BJ, Sole AJ, Cowton TR, Lea JM, Slater DA, Fahrner D and Nienow PW (2020) Subglacial drainage evolution modulates seasonal ice flow variability of three tidewater glaciers in southwest Greenland. *Journal of Geophysical Research: Earth Surface* 125(9): e2019JF005492.

Dokken TM and Jansen E (1999) Rapid changes in the mechanism of ocean convection during the last glacial period. *Nature* 401(6752): 458–461.

Dyke LM, Andresen CS, Seidenkrantz M-S et al. (2017) Minimal Holocene retreat of large tidewater glaciers in Køge Bugt, southeast Greenland. *Scientific Reports* 7: 2330.

Dyke LM, Hughes AL, Murray T, Hiemstra JF, Andresen CS and Rodés Á (2014) Evidence for the asynchronous retreat of large outlet glaciers in southeast Greenland at the end of the last glaciation. *Quaternary Science Reviews* 99: 244–259.

Ekblom Johansson F, Wangner DJ, Andresen CS et al. (2020) Glacier and ocean variability in Ata Sund, west Greenland, since 1400 CE. *The Holocene* 30(12): 1681–1693.

Enderlin EM, Carrigan CJ, Kochtitzky WH, Cuadros A, Moon T and Hamilton GS (2018) Greenland iceberg melt variability from high-resolution satellite observations. *The Cryosphere* 12(2): 565–575.

Erbs-Hansen DR, Knudsen KL, Olsen J et al. (2013) Paleoceanographical development off Sisimiut, West Greenland, during the mid- and late Holocene: A multiproxy study. *Marine Micropaleontology* 102: 79–97.

Fenty I, Willis JK, Khazendar A, Dinardo S, Forsberg R, Fukumori I, Holland D, Jakobsson M, Moller D, Morison J, Münchow A, Rignot E, Schodlok M, Thompson AF, Tinto K, Rutherford M and Trenholm N (2016) Oceans Melting Greenland: Early results from NASA's ocean-ice mission in Greenland. *Oceanography* 29(4): 72–83.

Fronval T, Jansen E, Bloemendal J et al. (1995) Oceanic evidence for coherent fluctuations in Fennoscandian and Laurentide ice sheets on millennium timescales. *Nature* 374: 443–446.

Funder S, Hjort C, Landvik JY et al. (1998) History of a stable ice margin—East Greenland during the middle and upper Pleistocene. *Quaternary Science Reviews* 17(1–3): 77–123.

Funder S, Kjeldsen KK, Kjær KH and Cofaigh CÓ (2011) The Greenland Ice Sheet during the past 300,000 years: A review. *Developments in Quaternary Sciences* 15: 699–713.

Grimm EC (1987) Coniss: A Fortran 77 program for stratigraphically constrained cluster analysis by the method of incremental sum of squares. *Computational Geosciences* 13: 13–35.

Häkkinen S, Rhines PB and Worthen DL (2011) Atmospheric blocking and Atlantic multidecadal ocean variability. *Science* 334: 655–659.

Hansen KE, Giraudeau J, Wacker L et al. (2020) Reconstruction of Holocene oceanographic conditions in eastern Baffin Bay. *Climate of the Past* 16: 1075–1095.

Hasle GR and Syvertsen EE (1997) Marine diatoms. In: Tomas CR (ed.) *Identifying Marine Phytoplankton*. San Diego, CA: Academic Press, pp.5–385.

Hatun H, Sando AB, Drange H et al. (2005) Influence of the Atlantic subpolar gyre on the thermohaline circulation. *Science* 309: 1841–1844.

Heaton TJ, Köhler P, Butzin M et al. (2020) Marine20—The marine radiocarbon age calibration curve (0–55,000 Cal BP). *Radiocarbon* 62(4): 779–820.

Henriksen N and Higgins AK (2009) Descriptive text to Geological map of Greenland, 1: 500 000, Dove Bugt, Sheet 10. *Geological Survey of Denmark and Greenland Map Series* 4: 1–32.

Holland DM, Thomas RH, de Young B et al. (2008) Acceleration of Jakobshavn isbræ triggered by warm subsurface ocean waters. *Nature Geoscience* 1: 659–664.

Howat IM, Negrete A and Smith BE (2014) The Greenland Ice mapping Project (GIMP) land classification and surface elevation data sets. *The Cryosphere* 8: 1509–1518.

Hughes ALC, Rainsley E, Murray T et al. (2012) Rapid response of Helheim glacier, southeast Greenland, to early Holocene climate warming. *Geology* 40(5): 427–430.

Inall ME, Murray T, Cottier FR et al. (2014) Oceanic heat delivery via Kangerdlugssuaq Fjord to the south-east Greenland ice sheet. *Journal of Geophysical Research: Oceans* 119: 631–645.

IPCC (2021) *Climate Change 2021: The Physical Science Basis. Contribution of Working Group I to the Sixth Assessment Report of the Intergovernmental Panel on Climate Change*. Cambridge: Cambridge University Press.

Jackson RH, Straneo F and Sutherland DA (2014) Externally forced fluctuations in ocean temperature at Greenland glaciers in non-summer months. *Nature Geoscience* 7: 503–508.

Jaeger JM and Koppes MN (2015) The role of the cryosphere in source-to-sink systems. *Earth-Science Reviews* 153: 43–76.

Jennings A, Andrews J and Wilson L (2011) Holocene environmental evolution of the SE Greenland shelf north and south of the Denmark strait: Irminger and East Greenland current interactions. *Quaternary Science Reviews* 30: 980–998.

Jennings A, Weiner N, Helgadottir G et al. (2004) Modern foraminiferal faunas of the southwestern to northern Iceland shelf: Oceanographic and environmental controls. *Journal of Foraminiferal Research* 34: 180–207.

Jennings AE, Bailey E, Oliver B et al. (2015) Retreat of the coalescent Greenland and Innuitian ice sheets from Nares Strait. In: *AGU fall meeting abstracts*, Vol. 2015, pp.PP51C–2305. Washington, DC: American Geophysical Union.

Jennings AE, Hald M, Smith M et al. (2006) Freshwater forcing from the Greenland ice sheet during the younger dryas:

Evidence from southeastern Greenland shelf cores. *Quaternary Science Reviews* 25: 282–298.

Jennings AE and Helgadottir G (1994) Foraminiferal assemblages from the fjords and shelf of eastern Greenland. *Journal of Foraminiferal Research* 24: 123–144.

Jennings AE, Knudsen KL, Hald M et al. (2002) A mid-Holocene shift in Arctic sea-ice variability on the East Greenland shelf. *The Holocene* 12(1): 49–58.

Jiang H, Muscheler R, Björck S et al. (2015) Solar forcing of Holocene summer sea-surface temperatures in the northern North Atlantic. *Geology* 43(3): 203–206.

Jiang H, Seidenkrantz M-S, Knudsen KL et al. (2001) Diatom surface sediment assemblages around Iceland and their relationships to oceanic environmental variables. *Marine Micropaleontology* 41: 73–96.

Justwan A and Koç N (2009) Evolution of the East Greenland Current between 1150 and 1740 AD, revealed by diatom-based sea surface temperature and sea-ice concentration reconstructions. *Polar Research* 28(2): 165–176.

Kjeldsen KK, Korsgaard NJ, Bjørk AA et al. (2015) Spatial and temporal distribution of mass loss from the Greenland ice sheet since AD 1900. *Nature* 528: 396–400.

Koc Karpuz N and Schrader H (1990) Surface sediment diatom distribution and Holocene paleotemperature variations in the Greenland, Iceland and Norwegian Sea. *Paleoceanography* 5: 557–580.

Korsgaard NJ, Nuth C, Khan SA et al. (2016) Digital elevation model and orthophotographs of Greenland based on aerial photographs from 1978–1987. *Scientific Data* 3: 1–15.

Krissek LA (1989) (Table 2) Sampling intervals and ages of ODP Hole 104-642B. doi:10.1594/PANGAEA.736321, in Supplement to: Krissek, L.A. 1989: Late Cenozoic records of ice-rafting at ODP Sites 642, 643, and 644, Norwegian Sea: Onset, chronology, and characteristics of glacial/interglacial fluctuations. In: Eldholm O, Thiede J, Taylor E, et al. (eds) *Proceedings of the Ocean Drilling Program, Scientific Results*. College Station, TX: Texas A&M University, pp.61–74.

Larocca LJ, Axford Y, Bjørk AA et al. (2020a) Local glaciers record delayed peak Holocene warmth in south Greenland. *Quaternary Science Reviews* 241: 106421.

Larocca LJ, Axford Y, Woodroffe SA et al. (2020b) Holocene glacier and ice cap fluctuations in southwest Greenland inferred from two lake records. *Quaternary Science Reviews* 246: 106529.

Larsen NK, Kjær KH, Olsen J et al. (2011) Restricted impact of Holocene climate variations on the southern Greenland ice sheet. *Quaternary Science Reviews* 30: 3171–3180.

Larsen NK, Strunk A, Levy LB et al. (2017) Strong altitudinal control on the response of local glaciers to Holocene climate change in southwest Greenland. *Quaternary Science Reviews* 168: 69–78.

Lecavalier BS, Milne GA, Vinther BM et al. (2013) Revised estimates of Greenland ice sheet thinning histories based on ice-core records. *Quaternary Science Reviews* 63: 73–82.

LeGrande AN and Schmidt GA (2008) Ensemble, water isotope-enabled, coupled general circulation modeling insights into the 8.2 ka event. *Paleoceanography* 23: PA3207.

Levy LB, Kelly MA, Lowell TV, Hall BL, Hempel LA, Honsaker WM, Lusas AR, Howley JA and Axford YL (2014) Holocene fluctuations of Bregne ice cap, Scoresby Sund, east Greenland: a proxy for climate along the Greenland Ice Sheet margin. *Quaternary Science Reviews* 92: 357–368.

Lohmann J and Ditlevsen PD (2021) Risk of tipping the overturning circulation due to increasing rates of ice melt. *Proceedings of the National Academy of Sciences of the United States of America* 118: e2017989118.

Lowell TV, Hall BL, Kelly MA et al. (2013) Late Holocene expansion of Istorvet ice cap, Liverpool Land, east Greenland. *Quaternary Science Reviews* 63: 128–140.

McManus JF, Oppo DW and Cullen JL (1999) A 0.5-million-year record of millennial-scale climate variability in the North Atlantic. *Science* 283(5404): 971–975.

Medlin LK and Priddle J (1990) *Polar Marine Diatoms*. Cambridge: Natural Environment Research Council.

Mienert J, Andrews JT and Milliman JD (1992) The East Greenland continental margin (65°N) since the last deglaciation: Changes in seafloor properties and ocean circulation. *Marine Geology* 106(3–4): 217–238.

Miettinen A, Divine DV, Husum K et al. (2015) Exceptional ocean surface conditions on the SE Greenland shelf during the medieval climate anomaly. *Paleoceanography* 30: 1657–1674.

Millan R, Rignot E, Mouginot J, Wood M, Bjørk AA and Morlighem M (2018) Vulnerability of southeast greenland glaciers to warm atlantic water from operation icebridge and ocean melting greenland data. *Geophysical Research Letters* 45(6): 2688–2696.

Moon T, Joughin I, Smith B et al. (2012) 21st-Century evolution of Greenland outlet glacier velocities. *Science* 336: 576–578.

Morlighem M, Rignot E, Mouginot J et al. (2014) Deeply incised submarine glacial valleys beneath the Greenland ice sheet. *Nature Geoscience* 7: 418–422.

Moros M, Jensen KG and Kuijpers A (2006) Mid-to late-Holocene hydrological and climatic variability in Disko Bugt, central West Greenland. *The Holocene* 16: 357–367.

Mugford RI and Dowdeswell JA (2010) Modeling iceberg-rafted sedimentation in high-latitude fjord environments. *Journal of Geophysical Research* 115: F03024.

Murray JW (1991) *Ecology and Palaeoecology of Benthic Foraminifera*. Harlow: Longman Scientific & Technical; New York: Wiley.

NSIDC (National Snow and Ice Data Centre) (2012) Atlas of the Cryosphere.

Pados-Dibattista T, Pearce C, Detlef H et al. (2022) Holocene palaeoceanography of the northeast Greenland shelf. *Climate of the Past* 18(1): 103–127.

Perner K, Moros M, Lloyd JM et al. (2015) Mid to late Holocene strengthening of the East Greenland current linked to warm subsurface Atlantic water. *Quaternary Science Reviews* 129: 296–307.

Polyakova YI (2001) Late Cenozoic evolution of northern Eurasian marginal seas based on the diatom record. *Polarforschung* 69: 211–220.

Quadfasel D, Gascard JC and Koltermann KP (1987) Large-scale oceanography in Fram Strait during the 1984 marginal ice zone experiment. *Journal of Geophysical Research Oceans* 92: 6719–6728.

Ran L, Jiang H, Knudsen KL et al. (2011) Diatom-based reconstruction of palaeoceanographic changes on the north Icelandic shelf during the last millennium. *Palaeogeography, Palaeoclimatology, Palaeoecology* 302: 109–119.

Reimer PJ, Bard E, Bayliss A et al. (2013) IntCal13 and Marine13 radiocarbon age calibration curves 0–50,000 years cal BP. *Radiocarbon* 55(4): 1869–1887.

Rignot E, Koppes M and Velicogna I (2010) Rapid submarine melting of the calving faces of West Greenland glaciers. *Nature Geoscience* 3: 187–191. https://doi.org/10.1038/ngeo765

Robel AA, Roe GH and Haseloff M (2018) Response of marine-terminating glaciers to forcing: time scales, sensitivities, instabilities, and stochastic dynamics. *Journal of Geophysical Research: Earth Surface* 123(9): 2205–2227.

Rosenau R, Scheinert M and Dietrich R (2015) A processing system to monitor Greenland outlet glacier velocity variations at decadal and seasonal time scales utilizing the Landsat imagery. *Remote Sensing of Environment* 169: 1–19.

Ruddiman WF (1977) Late quaternary deposition of ice-rafted sand in the subpolar North Atlantic (lat 40° to 65°N). *Geological Society of America Bulletin* 88(12): 1813–1827.

Rudels B, Jones EP, Anderson LG et al. (1994) On the intermediate depth waters of the Arctic Ocean. In: Johannessen OM, Muench RD and Overland JE (eds) *The Polar Oceans and Their Role in Shaping the Global Environment*. Washington, DC: American Geophysical Union (AGU), pp.33–46.

Sarafanov A (2009) On the effect of the North Atlantic Oscillation on temperature and salinity of the subpolar North Atlantic intermediate and deep waters, ICES. *Journal of Marine Science* 66(7): 1448–1454.

Schaffer J, von Appen W-J, Dodd PA et al. (2017) Warm water pathways toward Nioghalvfjerdsfjorden glacier, northeast Greenland. *Journal of Geophysical Research: Oceans* 122: 4004–4020.

Schoof C (2007) Ice sheet grounding line dynamics: Steady states, stability, and hysteresis. *Journal of Geophysical Research: Earth Surface* 112(F3).

Sciascia R, Straneo F, Cenedese C et al. (2013) Seasonal variability of submarine melt rate and circulation in an East Greenland fjord. *Journal of Geophysical Research: Oceans* 118: 2492–2506.

Seidenkrantz M-S (1995) *Cassidulina teretis*Tappan and *Cassidulina neoteretis* new species (Foraminifera): Stratigraphic markers for deep sea and outer shelf areas. *Journal of Micropalaeontology* 14: 145–157.

Seidenkrantz MS, Ebbesen H, Aagaard-Sørensen S, Moros M, Lloyd JM, Olsen J, Knudsen MF and Kuijpers A (2013) Early Holocene large-scale meltwater discharge from Greenland documented by foraminifera and sediment parameters. *Palaeogeography, Palaeoclimatology, Palaeoecology* 391: 71–81.

Sha L, Jiang H and Knudsen KL (2012) Diatom evidence of climatic change in Holsteinsborg dyb, west of Greenland, during the last 1200 years. *The Holocene* 22: 347–358.

Sha L, Jiang H, Liu Y et al. (2015) Palaeo-sea-ice changes on the north Icelandic shelf during the last millennium: Evidence from diatom records. *Science China Earth Sciences* 58: 962–970.

Sha L, Jiang H, Seidenkrantz M-S et al. (2014) A diatom-based sea-ice reconstruction for the Vaigat Strait (Disko Bugt, West Greenland) over the last 5000yr. *Palaeogeography, Palaeoclimatology, Palaeoecology* 403: 66–79.

Sha L, Jiang H, Seidenkrantz M-S et al. (2016) Solar forcing as an important trigger for West Greenland sea-ice variability over the last millennium. *Quaternary Science Reviews* 131: 148–156.

Sha L, Jiang H, Seidenkrantz M-S et al. (2017) A record of Holocene sea-ice variability off West Greenland and its potential forcing factors. *Palaeogeography, Palaeoclimatology, Palaeoecology* 475: 115–124.

Sheldon CM, Seidenkrantz M-S, Frandsen P et al. (2015) Variable influx of West Greenland Current water into the Labrador Current through the last 7200 years – A multiproxy record from Trinity Bay (NE Newfoundland). *Arktos – Arctic Geoscience* 1: 8.

Sheldon CM, Seidenkrantz M-S, Pearce C et al. (2016) Holocene oceanographic changes in SW Labrador Sea, off Newfoundland. *The Holocene* 26(2): 274–289.

Smith LM and Andrews JT (2000) Sediment characteristics in iceberg dominated fjords, Kangerlussuaq region, East Greenland. *Sedimentary Geology* 130(1–2): 11–25.

St. John KEK and Krissek LA (1999) Ice-rafted debris flux in the North Pacific from core 145-887. doi:10.1594/PANGAEA.738228, in supplement to: St. John, KEK; Krissek, LA (1999): Regional patterns of pleistocene ice-rafted debris flux in the North Pacific. *Paleoceanography* 14(5): 653–662.

Stoermer EF and Smol JP (1999) *The Diatom: Applications for the Environmental and Earth Sciences*. New York, NY: Cambridge University Press, p.469.

Straneo F, Hamilton GS, Sutherland DA et al. (2010) Rapid circulation of warm subtropical waters in a major glacial fjord in East Greenland. *Nature Geoscience* 3: 182–186.

Straneo F and Heimbach P (2013) North Atlantic warming and the retreat of Greenlands outlet glaciers. *Nature* 504: 36–43.

Sutherland DA and Pickart RS (2008) The East Greenland coastal current: Structure, variability, and forcing. *Progress in Oceanography* 78: 58–77.

Sutherland DA, Straneo F and Pickart RS (2014) Characteristics and dynamics of two major Greenland glacial fjords. *Journal of Geophysical Research Oceans* 119: 3767–3791.

Swift DA, Nienow PW, Spedding N et al. (2002) Geomorphic implications of subglacial drainage configuration: Rates of basal sediment evacuation controlled by seasonal drainage system evolution. *Sedimentary Geology* 149: 5–19.

Syvertsen EE and Hasle GR (1984) *Thalassiosira bulbosa* Syvertsen, sp. Nov., an arctic marine diatom. *Polar Biology* 3: 167–172.

Syvitski JP and Shaw J (1995) Sedimentology and geomorphology of fjords. In: Perillo GME (ed.) *Developments in Sedimentology*, vol. 53. Amsterdam: Elsevier, pp.113–178.

Thornalley DJR, Elderfield H and McCave N (2009) Holocene oscillations in temperature and salinity of the surface subpolar North Atlantic. *Nature* 457: 711–714.

Van Nieuwenhove N, Pearce C, Knudsen MF et al. (2018) Meltwater and seasonality influence on subpolar gyre circulation during the Holocene. *Palaeogeography, Palaeoclimatology, Palaeoecology* 502: 104–118.

Vermassen F, Andreasen N, Wangner DJ, Thibault N, Seidenkrantz MS, Jackson R, Schmidt S, Kjær KH and Andresen CS (2019a) A reconstruction of warm-water inflow to Upernavik Isstrøm since 1925 CE and its relation to glacier retreat. *Climate of the Past* 15(3): 1171–1186.

Vermassen F, Wangner DJ, Dyke LM, Schmidt S, Cordua AE, Kjær KH, Haubner K and Andresen CS (2019b) Evaluating ice-rafted debris as a proxy for glacier calving in Upernavik Isfjord, NW Greenland. *Journal of Quaternary Science* 34(3): 258–267.

Vinther BM, Buchardt SL, Clausen HB et al. (2009) Holocene thinning of the Greenland ice sheet. *Nature* 461(7262): 385–388.

von Quillfeldt CH (1996) *Ice algae and phytoplankton in north Norwegian and Arctic waters: Species composition, succession and distribution*. PhD Thesis, University of Tromsø, Norway.

von Quillfeldt CH (2000) Common diatom species in Arctic spring blooms: Their distribution and abundance. *Botanica Marina* 43(6): 499–551.

Wangner DJ, Jennings AE, Vermassen F, Dyke LM, Hogan KA, Schmidt S, Kjær KH, Knudsen MF and Andresen CS (2018) A 2000-year record of ocean influence on Jakobshavn Isbræ calving activity, based on marine sediment cores. *The Holocene* 28(11): 1731–1744.

Wangner DJ, Sicre MA, Kjeldsen KK, Jaeger JM, Bjørk AA, Vermassen F, Sha L, Kjær KH, Klein V and Andresen CS (2020) Sea surface temperature variability on the SE-Greenland Shelf (1796–2013 CE) and Its Influence on Thrym Glacier in Nørre Skjoldungesund. *Paleoceanography and Paleoclimatology* 35(3): e2019PA003692.

Witkowski A, Lange-Bertalot H and Metzeltin D (2000) Diatom flora of marine coasts. In: Lange-Bertalot H (ed.) *Iconographia diatomologica*. Liechtenstein: A.R.G. Gantner, pp.1–925.